**RESEARCH ARTICLE**

# Mitigation of tribocorrosion of metals in aqueous solutions by potential-enhanced adsorption of surfactants

**Chenxu LIU**[1], **Yu TIAN**[1], **Zulfiqar A. KHAN**[2], **Yonggang MENG**[1,2,*]

[1] *State Key Laboratory of Tribology in Advanced Equipment, Tsinghua University, Beijing 100084, China*

[2] *NanoCorr, Energy & Modelling Research Group, Bournemouth University, Bournemouth, UK*

© The author(s) 2022.

**Abstract:** Corrosion and corrosive wear occur commonly on metals surface in aqueous solutions. External electric field is usually considered as one of the factors to accelerate corrosion or corrosive wear of materials in the presence of conventional electrolytes. This work aims to reposition widely believed perspective by experimental justification which have been conducted in aqueous solutions containing surfactants. Electric potential of metal surfaces was modulated externally within the electrochemical potential window of the metal electrode-solution-counter electrode system, which actively regulated the adsorption or desorption of surfactant molecule in the aqueous solution over the electrodes to form a molecular barrier of electron transportation across the electrode–electrolyte interface. The advantage of the approach over the anodic passivation is negligible redox reactions on the protected electrode surface while a better lubricious and wear resistant film than oxide is maintained in the meantime. Tribopairs of several metal/metal and metal/ceramic were tested by employing a ball-on-disc tribometer with anionic and cationic surfactants solutions. For anionic surfactant as the modifier, positive surface potential enables coefficient of friction to be decreased by promoting the formation of adsorption film on metal surface in aqueous solutions. For cationic surfactant, negative surface potential plays a role in decreasing the coefficient of friction. Phase diagrams of friction and wear in wide ranges of surfactant concentration and surface potential were plotted for the tested metal/metal and metal/ceramic tribopairs. These results indicate that the adsorption behavior of molecules or ions at the metal–aqueous interface can be well regulated when an external electric field is present without inducing corrosion or corrosive wear.

**Keywords:** corrosive wear; metal; electric field; surfactant; adsorption

## 1 Introduction

Corrosion and tribocorrosion are common on metal surfaces in the environment of humid atmosphere and aqueous solutions. They are both dependent on the surface properties of the materials and environment. Besides of material's compositions, structure and surface coatings, the surface potential is also considered to be a key factor, the effects of which are either positive or negative on resistance of corrosion and tribocorrosion, depending on both the polarity and magnitude of the inherent or imposed electrical potential [1].

Previous studies have been mostly focused over the effects of applied potential on metal corrosion or corrosive wear and have been conducted at anodic potentials. In the absence of wear, the anodic oxidation technique is widely used in industry to protect metal surfaces from corrosion by forming a passivation layer [2, 3]. However, the friction behavior or corrosion-wear behavior of the passivation layer generally depends on its mechanical properties and structural characteristics. The role of oxide layer in

the wear of metals has been studied extensively in an oxygen-rich environment [4]. Abd-El-Kader and El-Raghby found that chemical reactions at anodic potentials could lead to a wear rate almost twice the wear rate at cathodic potentials [5]. They reported that corrosive wear could mainly be attributed to surface oxide film formation and its removal. Significantly higher wear rate of 316L austenitic stainless steel at passive potentials was also reported by Favero et al., in their sliding experiments against alumina under electrochemical control in sulfuric acid [6]. The findings may be explained by the presence of the passive film, which can induce residual stress and interfere with dislocation activity. Tan et al. [7] summarized the effects of anodic potentials on corrosive wear as follows: (1) the broken oxide film produced abrasive particles which further accelerated wear-affected corrosion and enhanced mechanical wear; (2) the transmission of metal into oxides was beneficial for the tribofilm formation. In most cases, anodic potentials tend to accelerate the corrosive wear rate due to the formation and removal of the oxide film on the wear track of metals.

Studies on the corrosive wear of biomaterials have mostly focused on the pure mechanical wear component in tribocorrosion to minimize the effect of anodic oxidation at negative potentials [8]. Sun and Bailey [9] investigated the effect of cathodic potentials on the friction behavior of CoCrMo (a biomedical alloy) sliding against an $Al_2O_3$ slider in NaCl solution. They found that the coefficient of friction (COF) and total material loss decreased with an increasing cathodic potential, which may be attributed to hydrogen charging and hydrogen segregated layer formation on the alloy surface. Nevertheless, the influence of the cathodic potential is dependent on the type of materials. For CoCrMo alloy with S/Cr(C) coating in NaCl solution, a large amount of material is transferred to the slider at cathodic potentials, accelerating the mechanical wear of the coating [10]. Moreover, Akonko et al. [11] reported that hydrogen embrittlement was a non-ignorable phenomenon for metals at negative potentials. Their research demonstrated that cathodic protection under potentiostatic conditions was beneficial at a low frictional force, whereas it became ineffective under severe wear condition or at more negative cathodic potentials.

Corrosive wear also occurs due to current-carrying friction and charged lubrication. Sun et al. [12] investigated the tribological behavior of Cu/Cu rolling current-carrying contact pairs in a water-dripping condition. The results showed that the COF increased with the magnitude of applied current and peaked over 1.1 when the current was 1.5 A. Xie et al. [13] investigated the damage on lubricated surfaces in bearings with the passage of electrical current at 1 mA. Their results showed that many narrow and deep pits formed on the lubricated surfaces with polar glycerine as the lubricant, and microbubbles were considered to be responsible for the observed damage. Nevertheless, electric fields can also be used to accelerate the corrosive wear of materials for the purpose of a higher polishing efficiency [14]. Kulkarni et al. [15] investigated the electrochemical-mechanical wear behavior of copper during chemical mechanical polishing (CMP). They observed a marked effect on surface integrity after polishing with alternating potentials compared with anodic or cathodic potentials alone because the material was removed atomically through different oxidation states by alternating the electrical potential.

The findings of the studies mentioned above indicate that oxidation or reduction reactions occur on the electrode surface (both inside and outside the wear track), which lead to corrosive wear. The interplays between electric potentials and friction are more complicated than wear. In 1994, Zhu et al. [16] summarized the following four main mechanisms responsible for of the effect of applied electric fields or potentials on friction. The first mechanism is the production of gases resulted from the over electrochemical potential. The second one is the decrease in hardness of rubbing metals due to the electrochemical potential. The third one is the formation of adsorbed molecular layers on the surfaces under the electrochemical potential, and the last one is the electrochemical potential promoting or inhibiting redox reactions. After more than two decades, Spikes [17] further reviewed the effect of applied electrical potentials on the friction and wear of lubricated contacts, and concluded that the most important mechanisms are promotion of adsorption/desorption of polar additives on tribological surfaces and

stimulation or suppression of redox reactions involving either oxygen or lubricant additives at tribological surfaces. He proposed that applied potentials may enhance friction and increase wear, for example by suppressing the adsorption of additives on surfaces, oxidizing the rubbing surface rapidly, or generating undesirable species such as hydrogen. If they are deliberate and well-chosen, they may lead to more effective tribofilm formation. However, the association between the above mechanisms has not been clarified, and the appropriate method for achieving smart friction control by using the electric field remains unknown.

In the last two decades, there have been a series of studies on potential controlled friction for various solutions with or without additives of various kinds of surfactants, ionic liquid, nanoparticles, zinc dialkyldithiophosphate (ZDDP), and organic molybdenum [18]. In 1998, Jiang et al. [19] found that external voltages could increase the friction coefficient of $Al_2O_3$/Cu sliding pairs in an emulsion of 1 wt% zinc stearate dispersed in $H_2O$. The COF was increased from 0.15 to 0.45 at a voltage of 20 V when the lower specimen was used as the cathode. They suggested that the electric potential affected the friction by changing both the surface interactions and state of boundary films. In 2002, Chang et al. [20] found that the electrolysis of $H_2O$ was the key trigger to the change of COF in the presence of a sufficiently negative electric potential; in their study, the transition from low to high friction was coincident with that of the electrolysis of the solution. Controlling the process of friction in the above researches is typically accompanied by corrosion and corrosive wear as the applied potentials are higher than the hydrolysis potential of water. As a key step in understanding the potential controlled friction, He et al. [21] investigated friction behavior in the electrochemical window or non-faradaic electrochemical window. They reported that charge accumulation on the metal surface of the friction pair was a key factor that determined the adsorption/ desorption of surfactant ions, resulting in the decrease or increase of the COF. The response time of the COF to increase from 0.10 to 0.45 was less than 1.5 s when the potential was changed from the open circuit potential (OCP) to a negative value. Most recently, we investigated the effect of normal loads on the electrochemical window and found a difference in electrochemical reactions between the friction contact and non-contact areas [22]. It had been predicted that if the local external pressure was 1 GPa and the activation volume of metal atoms was 1 mol, the potential change caused by external force was around 20–40 mV. In most cases, especially when there are considerable amounts of adsorbed material (such as surfactant) in the electrolyte, the effect of pressure and shear force on the electrochemical window can be ignored.

Regardless of the presence of external forces, applying an external electric field can change the electrical potential of electrodes. The consensus among researchers is that electrochemical processes generally include adsorption/desorption when the applied surface potential is within the electrochemical potential window, reduction at negative potentials, and oxidation at positive potentials. Therefore, electrochemical reactions mainly occur on the metal surface when the surface potential is beyond the electrochemical window, which could result in relatively severe corrosion or corrosive wear. However, in the electrochemical window, the electrode surface mainly undergoes adsorption or desorption processes. The corrosion and corrosive wear behaviors of the metals are closely related to the properties of the adsorbed ions or charged particles.

Based on the current understanding of potential controlled friction and the electrochemical window, the effects of the external electric field on the corrosion and corrosive wear are discussed in this work. The distinctions between electrochemical reactions and the adsorption/desorption process are clarified. The relationship between friction behavior, surface potential, and concentration of the friction modifier is examined by plotting wear maps or friction maps of metal/metal or metal/ceramic tribopairs. The mechanism of the effects of potential-enhanced adsorption on corrosion and tribocorrosion is discussed in terms of molecular semiconductor physics. This work will not only demonstrate that an electric field can avoid the corrosion and corrosive wear of metals in aqueous solutions, but also present the design of material systems and surface potentials for the effective control of corrosion and corrosive wear.

## 2 Electrode processes and electrochemical potential window

For most electrode processes, charges are transferred across the solid–solution interface, causing oxidation or reduction to occur. The reactions are governed by Faraday's law [23]. Hence, such processes are generally called faradaic processes. Under some conditions, no charge-transfer reaction occur because such reactions are thermodynamically or kinetically unfavorable. However, adsorption and desorption processes can occur, and external currents can flow when the potential, electrode area, or solution composition changes. These processes are called non-faradaic processes [23].

Electrochemical potential window in current–voltage curve is usually used to briefly distinguish the non-faradaic processes with the faradaic processes. When applied surface potential is within the electrochemical potential window, adsorption and desorption of ions or molecules, instead of oxidation or reaction occur. Although the faradaic processes are usually of primary interest in the investigation of an electrode reaction, the non-faradaic processes must be also considered during the charge transfer and associated reactions. Non-faradaic processes can exist alone, while faradaic processes must co-exist with non-faradaic processes [23].

Material scientists and tribologists generally regard external electric field as the main cause of accelerated corrosion or corrosive wear of metals. However, this viewpoint is bias. In addition to the formation of corrosion resistant passivation film or tribo-electrochemical reaction film during the faradaic processes, the adsorption and desorption in the non-faradaic processes can also greatly affect the corrosion or corrosive wear behaviors, and even realize the active control of the corrosion and friction of the metals. Consequently, we focus on solid–solution interface where only non-faradaic processes occur.

To study the adsorption and desorption during the non-faradaic processes, electrical double layer model should be discussed firstly. In 1879, Helmholtz [24, 25] explained qualitatively the electrical properties of colloids on the concept of electrical double layer at solid–liquid interface. The model of Helmholtz is analogous to an electrical capacitor. The model provides a basis for rationalizing the electrical properties of the solid–liquid interface, while it does not account for thermal movement of ions in solution. A later model put forward by Gouy and Chapman, also named as diffused double layer model included the influence of the electrostatic interactions among ions and their thermal motion [23]. Stern [26] further improved the model by considering the size of ions and the solvated ions.

Up to now, the solution side of the electrical double layer is generally thought to be made up of several layers. The inner layer, that closest to the electrode, contains solvent molecules and sometimes other species (ions or molecules) that are said to be specifically adsorbed. The locus of the electrical centers of the specially adsorbed ions is called the inner Helmholtz plane. Solvated ions can approach the metal only to a certain distance (less than their radius). The locus of centers of these nearest solvated ions is called the outer Helmholtz plane. The interaction of the solvated ions with the charged metal involves only long-range electrostatic forces [23]. These ions are said to be nonspecifically adsorbed. Because of thermal agitation in the solution, the nonspecifically adsorbed ions are distributed in a three dimensional region called the diffuse layer [23].

The structure of the double layer can not only affect the rates of electrode processes, but also influence the boundary lubrication behavior of tribo-pairs especially in aqueous solution.

To better understand the nature of electrochemical potential window and the response of boundary lubrication to electric field, the double-layer capacitance and charging current should be considered priority. Here we use the simplest parallel plate capacitor, according to the Helmholtz model, to discuss the charging process and charging current of a double layer.

For non-faradaic processes, the behavior of the electrode–solution interface is analogous to that of a capacitor [23]. When an external potential is applied to the capacitor, the charge accumulates on the two plates of the capacitor. This can be also regarded as a charging process. Its behavior is governed by Eq. (1):

$$C_d = \frac{q}{E_c} \tag{1}$$

where $q$ is the charge on the capacitor, $E_c$ is the potential step of the capacitor and $C_d$ is the capacitor between the solid–liquid interface.

During the process, the sum of the voltages, $E_R$ and $E_c$, across the resistor and the capacitor, respectively, equal to the applied potential step of magnitude $E$ [23]. Hence

$$E = E_R + E_c = i \cdot R_s + \frac{q}{C_d} \qquad (2)$$

where $R_s$ represents the solution resistance, $i$ denotes current and can be expressed by

$$i = \frac{dq}{dt} \qquad (3)$$

Combining Eqs. (2) and (3), we can obtain the relationship between $q$ and $t$ as

$$\frac{dq}{dt} = -\frac{q}{R_s \cdot C_d} + \frac{E}{R_s} \qquad (4)$$

Equation (4) is a first order non-homogeneous linear differential equation. To solve the equation, we can replace $\frac{E}{R_s}$ with 0 and obtain

$$\frac{dq}{dt} + \frac{q}{R_s \cdot C_d} = 0 \qquad (5)$$

Equation (5) has a solution of the form

$$q = C_1 \cdot e^{-\int \frac{1}{R_s \cdot C_d} dt} \qquad (6)$$

where $C_1$ is a constant.

Here, a method of constant variation is used to solve the general solution of the Eq. (4), by substituting the constant $C_1$ in Eq. (6) for $\mu(t)$ as

$$q = \mu(t) \cdot e^{-\int \frac{1}{R_s \cdot C_d} dt} \qquad (7)$$

Differentiating Eq. (7) with respect to $t$, we obtain

$$\frac{dq}{dt} = \mu'(t) \cdot e^{-\int \frac{1}{R_s \cdot C_d} dt} - \frac{\mu(t)}{R_s \cdot C_d} \cdot e^{-\int \frac{1}{R_s \cdot C_d} dt} \qquad (8)$$

Substituting Eqs. (7) and (8) into Eq. (4), we obtain

$$\mu'(t) = \frac{E}{R_s} \cdot e^{\int \frac{1}{R_s \cdot C_d} dt} \qquad (9)$$

Thus

$$\mu(t) = \int \frac{E}{R_s} \cdot e^{\int \frac{1}{R_s \cdot C_d} dt} \cdot dt + C_2 \qquad (10)$$

Substituting Eq. (10) into Eq. (9), we obtain

$$q = \left( \int \frac{E}{R_s} \cdot e^{\int \frac{1}{R_s \cdot C_d} dt} \cdot dt + C_2 \right) \cdot e^{-\int \frac{1}{R_s \cdot C_d} dt} \qquad (11)$$

$$q = E \cdot C_d + C_3 \cdot e^{-\frac{t}{R_s \cdot C_d}} \qquad (12)$$

where $C_2$ and $C_3$ are constants.

Assume that the capacitor is initially uncharged, $q = 0$ at $t = 0$ [23], then we obtain

$$q = E \cdot C_d \cdot \left( 1 - e^{-\frac{t}{R_s \cdot C_d}} \right) \qquad (13)$$

By differentiating Eq. (13) with respect to $t$, the expression of $i$ with respect to $t$ can be obtained as

$$i = \frac{dq}{dt} = \frac{E}{R_s} \cdot e^{-\frac{t}{R_s \cdot C_d}} \qquad (14)$$

According to Eq. (14), the charging current reaches its maximum when $t = 0$ (at the moment of a voltage step change), and then decreases exponentially [23]. This equation can be used to explain the exponential decline of current over time for stainless steel in aqueous solution with 1 mM sodium dodecyl sulfate (SDS) and 10 mM NaCl, when the surface potential was changed from –0.1 to +0.2 V at 0 s in our previous research [27]. Most importantly, according to Eq. (14), the nature of electrochemical potential window and the non-faradaic processes for adsorption and desorption can be well understood by the charging and discharging processes of the electrical double layer between the electrode and the solution.

The above electrode processes are discussed without the influence of external forces. In some working environments, pressure or shear force acts directly or indirectly on the electrode surface. As we know, the traditional electrochemical processes generally include

adsorption/desorption processes when the surface potential of electrode is within the electrochemical potential window, reduction process at negative and oxidation process at positive potentials. For the electrode processes with the influence of external forces, triboelectrochemical processes including friction-induced reduction, friction-inhibited reduction, friction-induced oxidation, and friction-inhibited oxidation should be involved [22]. Friction could affect the electrode processes, as well as the electrochemical potential window. Here, we named it as tribo-electrochemical potential window. The adsorption/desorption processes (also named as non-faradaic processes) mainly affect the adsorption boundary lubrication film, while the electrochemical or tribo-electrochemical reaction process (faradaic processes) mainly affect the formation of the tribofilm on the surface of the tribopairs.

# 3 Wear map under different surface potentials

To systematically study the effect of external electric fields on corrosive wear behaviors of metals in aqueous, the relationships among friction, wear and the surface potential as well as the concentration of the friction modifier are researched by plotting wear maps of metal/metal or metal/ceramic with surfactant solution as lubricant. A tribometer (UMT-3, Bruker, Gemany) with an electrochemical workstation (PGSTAT302N, Auto, Switzerland) was used for the friction tests as shown in Fig. 1(a). Ceramic balls ($ZrO_2$, $Si_3N_4$) or metal balls (304 stainless steel, bearing steel) with diameter of 6.35 mm were used as the upper friction pair. 304 stainless steel plate, 316L stainless steel plate, Cu or Pt plate (about 10 mm × 15 mm × 2 mm)

was used as the lower friction pair, and the roughness (Ra) of the plates was about 10 nm. The load applied on the ball-on-plate contact was 1 or 3 N. The elasticity modulus and hardness of materials used in this work were listed in Table 1. According to Hertzian contact model, the pressure was 560 MPa for 304 plate vs 304 ball, 544 MPa for Cu plate vs $ZrO_2$ ball, and 619 MPa for Pt plate vs. $ZrO_2$ ball, respectively. In addition, the friction tests were performed at the sliding speed of 7 mm/s over a 3.5 mm track. The reciprocating frequency was set at 1 Hz. All the tests were carried out at room temperature.

SDS (99%, Meryer) or hexadecyl trimethyl ammonium bromide (CTAB, 99%, Aladdin Industrial Corporation) was selected as the friction modifier in deionized water, with the concentration range of 0.001 to 100 mM. The surface potential of the lower friction pair was controlled by a three electrode system (as shown in Fig. 1(b)), with Ag/AgCl electrode as the reference electrode with $E_0$ = 0.2224 V relative to the standard hydrogen electrode. The Ag/AgCl electrode was placed close to the lower friction pair with a gap about 1 mm. An external titanium alloy plate (about 10 mm × 20 mm × 2 mm) was used as the counter electrode. After friction tests, the morphologies of the wear tracks were inspected on an optical microscope (Keyence, Japan). The wear volumes and wear rates of the lower friction pairs were measured by using a 3D optical surface profiler (NewView, ZYGOLamda, USA).

Figure 2 presents the friction and wear maps of 304 stainless steel plate and 304 ball as the friction pairs and SDS aqueous solutions with different concentrations as lubricant. The x-axis represents the surface potential of metal lower friction pair. The y-axis represents the SDS concentration in aqueous
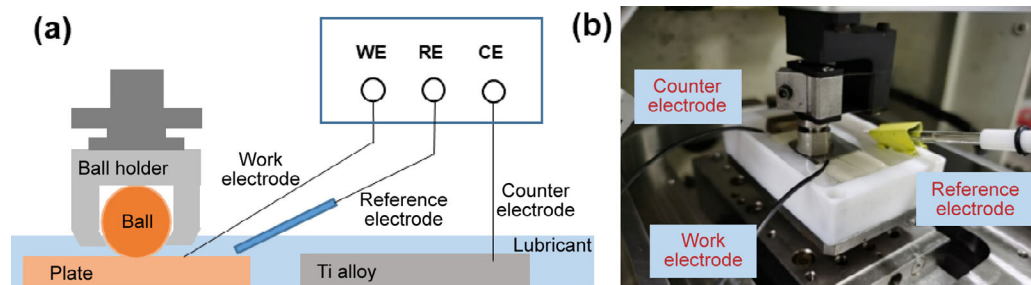


**Fig. 1** (a) Schematic diagram and (b) real picture of the tribometer combined with a three electrodes system.

**Table 1** Elasticity modulus and hardness of materials used in this work.

| Material | Elasticity modulus (GPa) | Hardness (GPa) |
|---|---|---|
| $ZrO_2$ | 245 | 16.2 |
| $Si_3N_4$ | 299 | 24.1 |
| Cu | 126 | 1.72 |
| Pt | 213 | 3.91 |
| 304 stainless steel | 174 | 4.70 |
| 316 stainless steel | 172 | 4.79 |

solution. Figures 2(a) and 2(b) show the COFs map and track widths map under different surface potentials and SDS concentrations drawn by Origin, respectively. According to the experimental values, different areas representing poor boundary lubrication state at low concentrations SDS solution, oxidation wear at low and high concentrations SDS solution, good boundary lubrication state and poor boundary lubrication state at high concentrations SDS solution are marked as A, B, C, D, and E respectively. Combining the results in Figs. 2(a) and 2(b), we tried to draw the friction and

wear map by Power Point, as shown in Fig. 2(c). For each coordinate position in Fig. 2(c), the dark color pattern represents the width of the track wear on the surface of the lower friction, while the light color pattern represents the friction coefficient. The area represents the size of the value. The entire circle represents a wear width of 240 μm, or a COF of 0.5. If the wear width is 120 μm or the COF is 0.25, the shape in that case will be a semicircle. The solid line in the figure represents a significant difference between the two states, while the dotted line represents an insignificant difference. Testing time for every condition in wear maps is 100 s.

When the SDS concentration is greater than 0.1 mM, the wear as well as the COF decrease with the increase of the surface potential of the 304 steel from negative to OCP (around 0.02 V). According to the previous studies, the DS$^-$ ions obtained by SDS dissociation in water play a major role in reducing the COF. At the negative potential, the electrostatic repulsion between the anion and plate surface causes the desorption of
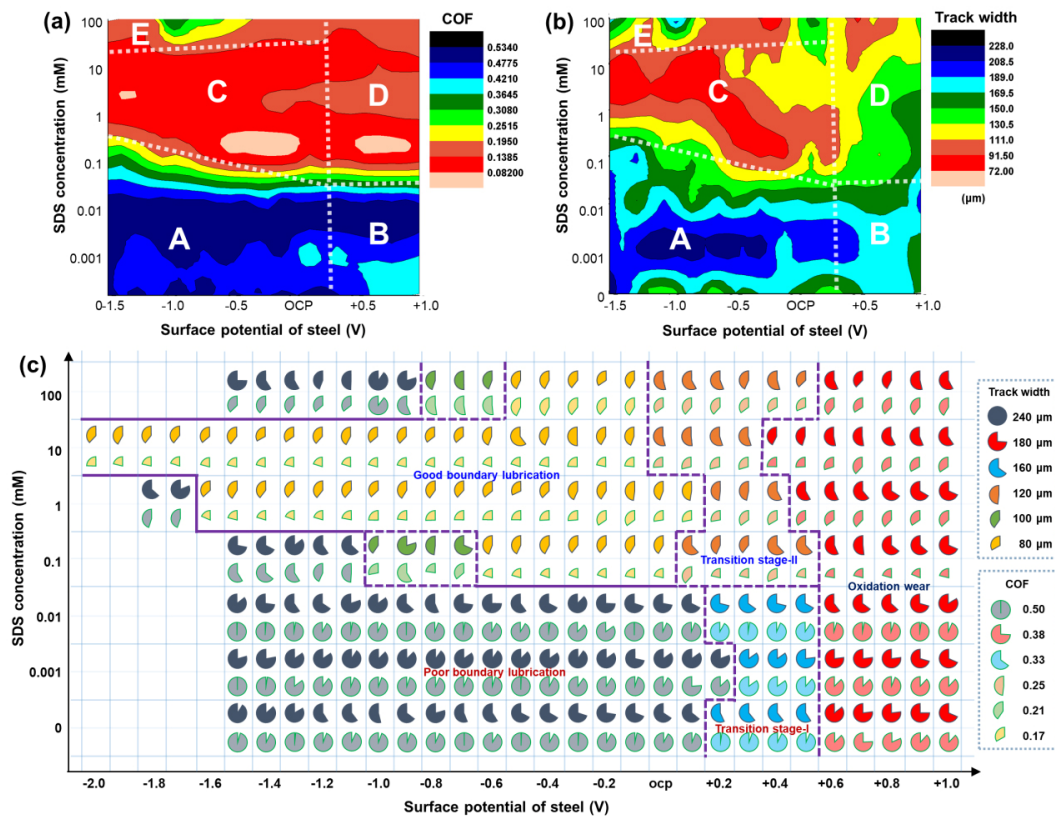


**Fig. 2** Friction and wear maps of 304/304 tribo-pairs lubricated with various concentrations of SDS aqueous solutions under different surface potentials. (a) COFs map and (b) track widths map under different surface potentials and SDS concentrations drawn by Origin, (c) friction and wear map drawn by Power Point.

DS⁻ on the plate surface. Under this condition, the COF is high and the friction interface is under a poor boundary lubrication state. When the surface potential is in the positive range, the COF will increase with the increase of the positive surface potentials, which is considered to be caused by the surface oxidation of the 304 stainless steel.

When the SDS concentration is low (≤ 0.01 mM), the addition of SDS is not enough to form a good boundary lubrication film on the surface of the friction pairs, causing the serious wear and a large COF. The micromorphologies of the wear tracks are shown in Fig. 3. As the SDS concentration increases to 1 mM, both of the wear width and the COF decrease. However, with the further increase of the SDS concentration (higher than the critical micelle concentration (CMC) of SDS), the COF obtained under OCP increases. Zhang and Meng [28] had reported the similar results in their research. They pointed that the adsorbed SDS molecules were in the form of monomers at the concentrations of 0.01, 0.1, and 1 mM, but formed regular hemimicelles at the concentration of 10 mM. The similar result has been observed in this work. At the same surface potential, the friction behavior of the boundary lubrication is worse for the case of 100 mM SDS than that of 10 or 1 mM SDS in the negative potential range.

Figure 3 presents some typical surface morphologies

of the wear tracks on 304 plate with different concentrations of SDS aqueous solutions (0.01–10 mM) as lubricant under different applied surface potentials, as the supplement information to Fig. 2. When the SDS concentration is 0.01 mM, severe wear occurred on the 304 surface. With the increase of the concentration at OCP, the wear condition becomes slight (for 0.1 mM SDS), then becomes serious (for 1 mM SDS or 10 mM SDS). The wear rate under the poor boundary lubrication (e.g. 0.01 mM SDS solution as lubricant, at −0.8 V or OCP) is $(1.212 \pm 0.433) \times 10^{-5}$ mm³/(N·m). For good boundary lubrication (e.g. 0.1 mM SDS or 1 mM SDS solution as lubricant, at −0.8 V or OCP), it is about $(3.262 \pm 0.791) \times 10^{-7}$ mm³/(N·m). When positive potential was applied, the wear rate becomes higher comparing with the condition at OCP. The wear rate is about $(1.772 \pm 0.283) \times 10^{-5}$ mm³/(N·m) for the 0.01 mM SDS as lubricant under +0.4 V or +0.8 V, about $(1.865 \pm 1.736) \times 10^{-6}$ mm³/(N·m) for the 1 mM SDS as lubricant. As discussed in Fig. 2, the relatively severe wear at the positive potential is mainly due to the oxidation of stainless steel.

304 stainless steel is prone to passivation in the anode region, which causes the mixed states or transition stages under the positive potentials, as marked by Transition stage-I and Transition stage-II in Fig. 2(c) when the surface potential is in the range of OCP to +0.5 V. In the second case, Cu plate was
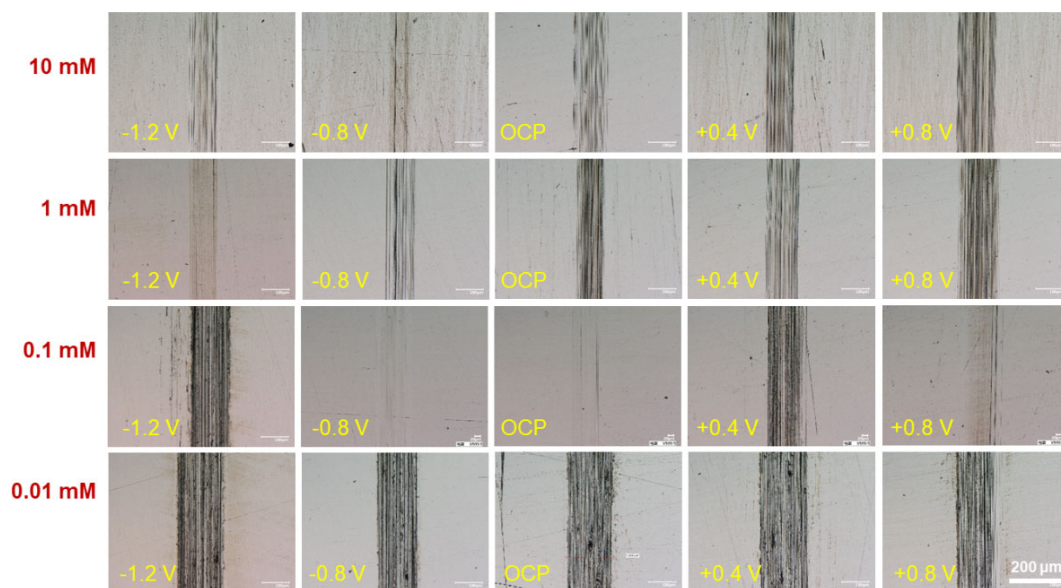


**Fig. 3** Surface morphologies of the wear tracks on 304 plate with different SDS aqueous solutions (0.01–10 mM) as lubrication under different applied surface potentials.

used as the lower friction and ZrO$_2$ ball as the upper friction. Comparing with the case of 304 stainless steel, it is more obvious to distinguish the oxidation wear and corrosive wear of Cu under positive potentials. Su [29] had reported that optimum boundary lubrication could be achieved during copper deformation, if the oxide thickness exceeded the minimum thickness of 6 nm and was composed of Cu$_2$O. The similar optimum boundary lubrication behaviors are also obtained in Fig. 4. With pure water or SDS solution with the concentration less than 10 mM as lubrication, tribofilm was formed on the surface of Cu without corrosion under the surface potential of +0.1 V. When the surface potential is higher than or equal to +0.2 V, corrosion can be observed on the surface of Cu. Owing to the existence of the oxidations in the wear track, the COF is relatively low when the surface potential is higher than +0.1 V with lower concentration SDS solutions as lubricant. For

the 100 mM SDS aqueous solution, no corrosion or oxidation film was observed on the surface of Cu plate. It is considered that the dense boundary adsorption film can inhibit the anodic reaction.

When the SDS concentration is in the range of 0.001–0.1 mM, the negative surface potential can increase the COF from ~0.1 to ~0.4. The effect of negative potentials on the friction behaviors of the Cu/ZrO$_2$ tribo-pairs is roughly similar to that of the 304/304 stainless steels. When the SDS concentration increases to 100 mM, the COFs decrease. The influence of the SDS concentration on the boundary lubrication of Cu/ZrO$_2$ is also similar to that of 304/304 steels and Ref. [28].

Figure 5 presents the surface morphologies of the wear tracks on Cu plate with different SDS aqueous solutions (1 or 0.01 mM) as lubrication under different applied surface potentials. For 0.01 mM SDS solution, the oxidation reaction of Cu mainly occurs in the
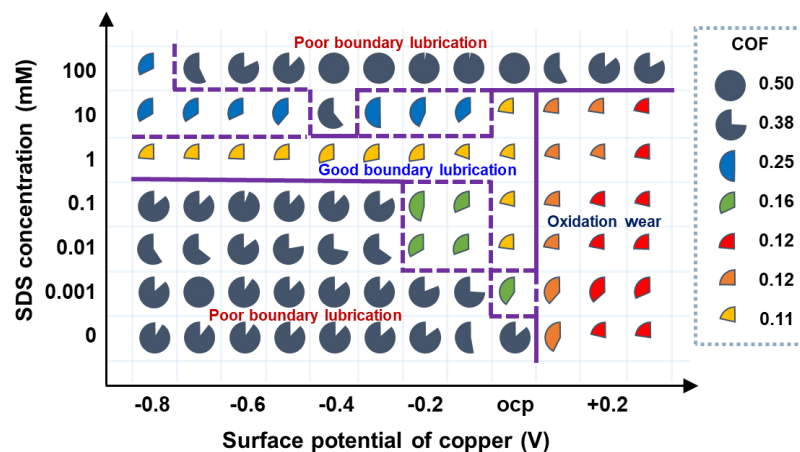


**Fig. 4** Friction map of Cu/ZrO$_2$ tribo-pairs lubricated with different concentrations of SDS aqueous solutions under different surface potentials.
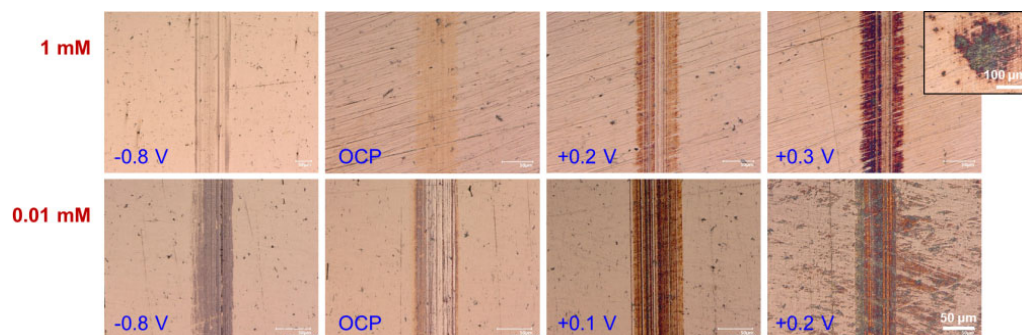


**Fig. 5** Surface morphologies of the wear tracks on Cu plate with different SDS aqueous solutions (1 or 0.01 mM) as lubrication under different applied surface potentials (the insert shows the morphologies near the track on the Cu plate at +0.3 V in 1 mM SDS solution after the friction test of 100 s).

wear track at 0.1 V. When the voltage increased to 0.2 V, obvious corrosion occurred on the whole Cu surface. For 1 mM SDS solution, the surface potential at which corrosion occurs on the Cu surface was about 0.3 V. These results also indicate that boundary adsorption film composed of SDS can inhibit the anodic reaction. Although the COFs as well as the surface morphologies of the wear tracks change greatly, the wear rates of the Cu plate at different surface potentials are $2\times10^{-6}$–$1.7\times10^{-5}$ mm³/(N·m).

In the third case, Pt was used as the lower friction pair and $ZrO_2$ ball as the upper friction pair. Owing to its chemical inertness, Pt is the better choice of material to research the adsorption and desorption behavior of ions or surfactants on its surface, comparing with stainless steel or Cu. At OCP, the COF decreases with the increase of the SDS concentration (Fig. 6). At

a certain positive potential, dark tribofilm can be observed in the wear track, which increases the COF obviously. For example, when the surface potential of the Pt plate is +0.4 V, the colors of the areas in- and outside of the wear track are almost the same. As the surface potential increases to +0.5 or +0.6 V, the color of the wear track becomes dark, as shown in Fig. 7. Correspondingly, the COF becomes higher. Different from 304 or Cu, there will be no corrosion on the surface of Pt, owing to its inertness.

For the case with 0.1 mM SDS aqueous as lubricant, the COF decreases under the positive potential of +0.2, +0.3, or +0.4 V. When the concentration of SDS is higher than 0.1 mM, the effect of surface potential becomes unobvious. The similar results can be found in the case of 10 mM in Fig. 2(c) and 1 mM in Fig. 4. These results indicate that it is difficult for the
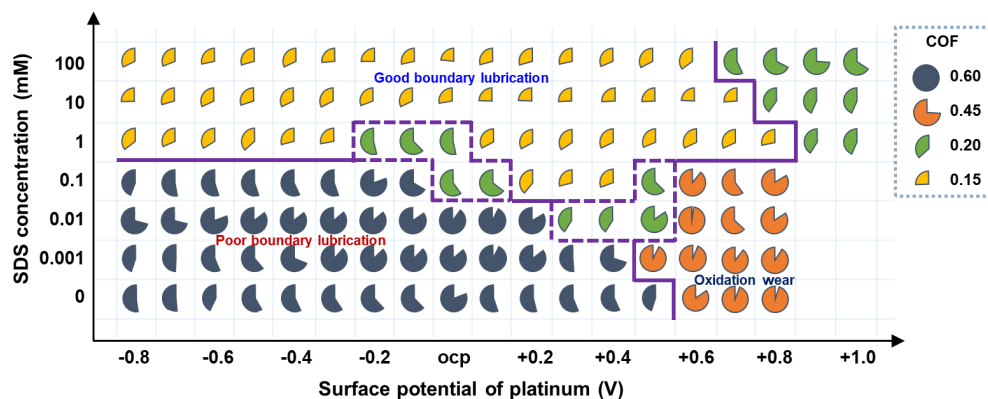


**Fig. 6** Friction behavior of Pt/ZrO₂ tribo-pairs lubricated with different concentrations of SDS aqueous solutions under different surface potentials.
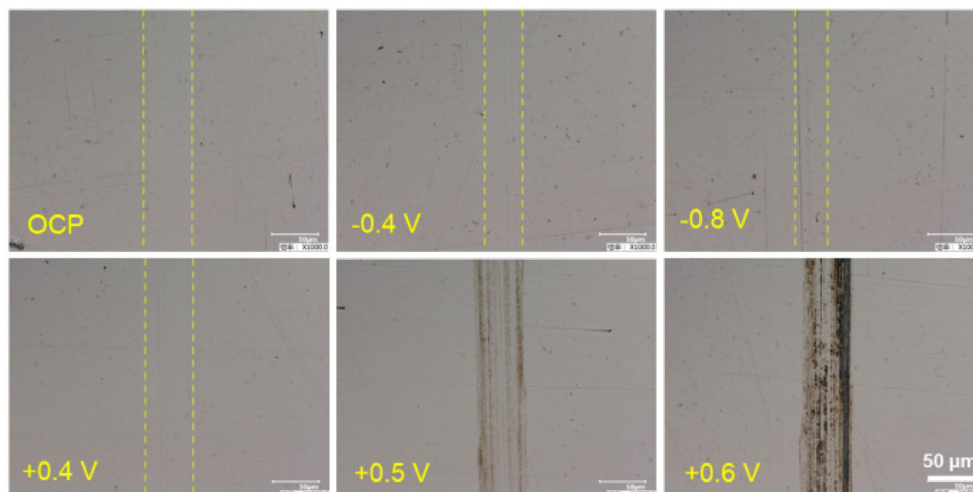


**Fig. 7** Surface morphologies of the wear tracks on Pt plate with 0.001 mM SDS aqueous solution as lubrication under different applied surface potentials.

surfactant to desorb from the surface of metal at high concentration. Moreover, when the SDS concentration is higher than 1 mM, there is no tribofilm formed in the track of the lower friction pair under the positive potentials. However, the COF is relatively high, which is consistent with the regularity in Fig. 4. When no oxidation wear occurs between Pt and ZrO$_2$ ball, the wear rate is about $2 \times 10^{-8}$–$6 \times 10^{-7}$ mm$^3$/(N·m), no matter for poor or good boundary lubrication. However, under certain positive potentials, a tribofilm on Pt surface grew up as a protrusion. The volume of the tribofilm can be measured with a 3D optical surface profiler (NewView, ZYGOLamda, USA). The formation rate of the tribofilm is about $1 \times 10^{-5}$–$6 \times 10^{-5}$ mm$^3$/(N·m) within 100 s, much higher than the wear rate.

According Figs. 2, 4, and 6, a wear map of metal/metal or metal/ceramic tribo-pairs lubricated with different concentrations of anionic surfactant aqueous under different surface potentials is summarized in Fig. 8 and described as follows.

Four lines (marked with I, II, III, and IV) crossing the *x*-axis correspond to five regions:

(1) Oxidation wear region. Electrochemical oxidation reaction takes place both in- and outside of the wear track of the lower friction pair. The types and structures of the oxides affect the tribological behaviors mostly. For example, CuO or CuO$_2$ can reduce the friction

coefficient [22, 29]. While, iron oxides increase the friction coefficient [7].

(2) Tribo-electrochemical oxidation region. Tribo-electrochemical reactions occur only inside of the track. The oxidation of Pt in electrochemical reaction in the absence of friction is difficult, owing that Pt electrode is not consumed during the reaction. However, under the action of force and positive potential, tribofilm composed of platinic oxide is formed, which increases the friction force during the test period.

(3) Electrochemical window region. Charging and discharging processes in electrochemical potential window can lead to the change of the adsorption mass as well as the transfer of the adsorption structures. Boundary lubrication can be controlled during this region by the active controlling of adsorption boundary film through electric field or surface potential without corrosion of metal.

(4) Tribo-electrochemical reduction region. It is almost the same with the tribo-electrochemical oxidation region, but occurs near the reduction reactions region. Friction force or pressure can change the critical surface potential at which reduction reactions occurs.

(5) Reduction reactions region. H$_2$ and OH$^-$ are formed by the electrolysis of water in this region. The OH$^-$ makes the pH value around the friction interface increase sharply. Under such alkali solution, the
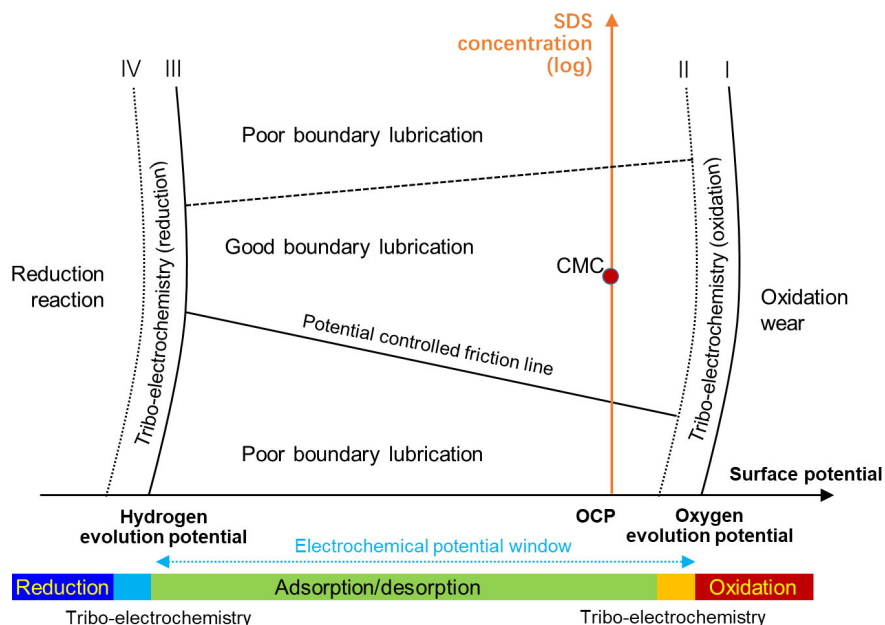


**Fig. 8** Schematic diagram combining the electrode processes with the wear map of metal/metal or metal/ceramic tribo-pairs lubricated with different concentrations of anionic surfactant (e.g., SDS) aqueous solutions under different surface potentials.

lubricating film formed previously under the surfactant solution is cleaned [20].

The shape of curves of I, II, III, and IV in Fig. 8 is related to the SDS concentration. The adsorption film reduces the shear stress during the friction process and isolates the solution from the metal, which can hinder the triboelectrochemical reactions. Compared with pure water, when the concentration of the solutions is slightly lower than CMC (e.g., 1 mM SDS solution works as electrolyte and Pt plate as electrode), the critical surface potentials of oxidation and reduction move about 0.2 V towards positive potential. Actually, the changes of the critical surface potentials as well as the electrochemical window range are influenced by the surfactant adsorption state and configuration. When the SDS concentration is much higher than CMC (e.g., 100 mM SDS solution works as electrolyte and Pt plate as electrode), the changes of critical surface potentials becomes unobvious. It is consistent with the experimental results of the friction when the high concentration of SDS solution is used as lubricant.

In addition, two lines crossing the *y*-axis correspond to three regions. When the concentration of the anionic surfactant is lower than the CMC, the COF as well as wear will decrease with the concentration increasing. There will be a line between the poor boundary lubrication and good boundary lubrication. The significant area of potential controlled friction effect is near the line within the electrochemical window. Here, we defined it as potential controlled friction line. When the concentration further increases and exceeds CMC, the COF increases and the wear becomes

severe. The poor boundary lubrication is considered to be caused by charging the adsorption conformation of surfactant from monolayer or monomers to hemimicelles.

Besides the anionic surfactant of SDS, a kind of cationic surfactant, CTAB was selected as the friction modifier in aqueous solutions. Figure 9 presents the friction behavior of Pt/ZrO$_2$ tribo-pairs lubricated with different concentrations of CTAB solutions under different surface potentials. When the concentration of CTAB is relatively low (e.g., 0.001 mM), the COFs are almost the same with that obtained in pure water lubrication. The tribofilm on the track of lower friction pair can be observed when the positive surface potential is higher than +0.4 V, which can increase the COF obviously. With the increase of the CTAB concentration from 0 to 1 mM, the COFs decrease from 0.47 to ~0.14 at OCP. When the concentration further increases to 10 mM, the COFs are stable at 0.13–0.14. For the case of the CTAB concentration at 0.1 mM, the COF decreases from 0.17 at OCP to 0.14 at the potential lower than –0.2 V. When the concentration is higher than 0.1 mM, the effect of potential controlled boundary lubrication becomes inapparent. The main difference between the friction maps of the CTAB lubrication system (Fig. 9) and the SDS lubrication system (Fig. 6) is the position of the potential controlled friction line. Because negative surface potential can decrease the COF and wear for cationic surfactant.

A non-ionic surfactant, Triton X-100 (Shanghai Yuanye Bio-Technology Co., Ltd.) was selected as friction modifier. The friction results in Fig. 10 show
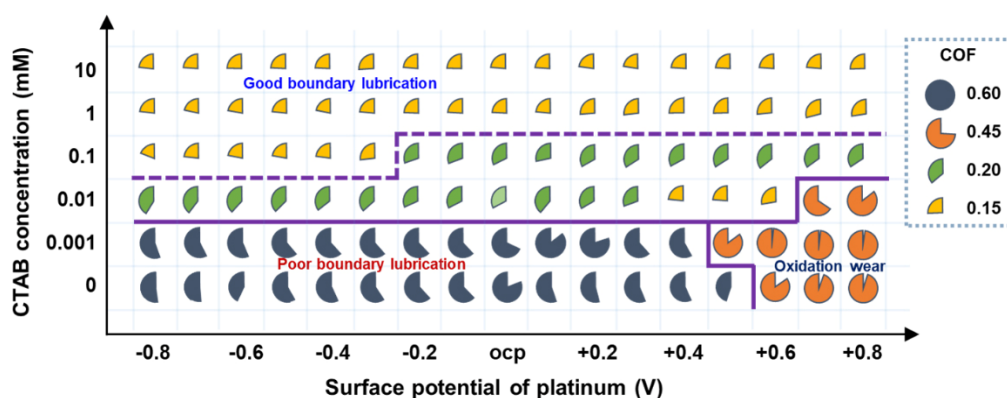


**Fig. 9** Friction map of Pt/ZrO$_2$ tribo-pairs lubricated with different concentrations of CTAB aqueous solutions under different surface potentials.
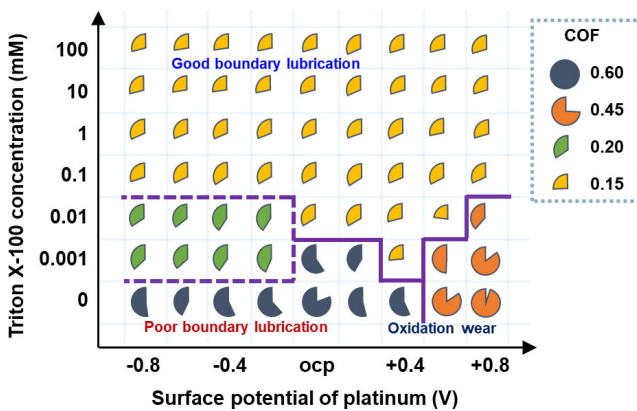
**Fig. 10** Friction map of Pt/ZrO₂ tribo-pairs lubricated with different concentrations of Triton X-100 aqueous solutions under different surface potentials.

that the COFs are around 0.16–0.17 with the concentration of Triton X-100 in the range of 0.01–100 mM, when the surface potential changes from –0.8 to +0.8 V. The potential controlled friction line is almost parallel to the *x*-axis for the non-ionic surfactant solutions.

## 4  Discussion

As shown in the wear maps under different surface potential, electrochemical reaction processes generally involve electrochemical corrosion, while the adsorption and desorption behaviors of ionic surfactants within the electrochemical potential window can realize the active control of friction without the corrosion of metals. Hence, it is necessary to discuss the structures and properties of adsorbed film under different surface potentials.

### 4.1  Adsorption behavior of surfactants under electric field

As a fundamental research, the adsorption capacity and state of surfactants at the solid–liquid interface are usually depended on instruments or methods. As introduced in Section 2, the capacity of the electrical double layer is a key parameter for the quantitative theory of the distribution of ions around a solid. In 1993, Sotiropoulos et al. [30] studied the adsorption of SDS from aqueous solutions on a polarized mercury electrode by means of differential capacitance measurements. Their results showed that at concentrations

below the CMC, two-dimensional aggregates were formed on the electrode surface within a polarization region which was bounded by two capacitance peaks at extreme positive and negative polarizations. The film was not particularly stable and was transformed into a compact layer at polarizations close to the potential of maximum adsorption.

In addition, direct molecular level experimental data were expected to show the adsorption configuration of surfactants on solid–solution interface. In 1995, images of surfactant aggregates at solid surfaces in aqueous solutions were obtained with atomic force microscopy (AFM) by Manne and Gaub [31]. The resulting structures for quaternary ammonium surfactants (above the CMC) were consistent with half-cylinders on crystalline hydrophobic substrates, full cylinders on mica, and spheres on amorphous silica. In 1999, Burgess et al. [32] presented the images of SDS at Au (111) by high-resolution scanning tunneling microscopy (STM). The adsorbed SDS formed strip-shaped hemimicellar aggregates at small or moderate charge densities at the electrode. The adsorbed SDS molecules were ordered and formed a long-range two-dimensional lattice. A unit cell of the lattice consisted of two vectors that were 4.4 and 0.5 nm long and were oriented at an angle of 70°. In 2001, the Gibbs surface excess of SDS as a function of electrode potential and the logarithm of the bulk SDS concentration was proposed and the thickness of the hemimicellar and condensed films were measured by neutron reflectivity experiments [33]. The properties of the condensed state were best explained by a model of an interdigitated film in which half of the sulfate groups were turned toward the metal and half toward the solution. In 2012, quantitative subtractively normalized interfacial Fourier transform infrared reflection spectroscopy (SNIFTIRS) was used to determine the conformation and orientation of SDS molecules adsorbed at the single crystal Au (111) surface [34]. The SDS molecules form a hemimicellar/ hemicylindrical structure for the range of potentials between −200 mV ≤ *E* < 450 mV and condensed film for electrode potentials ≥ 500 mV vs. Ag/AgCl. The SNIFTIRS measurements indicated that the alkyl chains within the two adsorbed states of SDS were in the liquid-crystalline state rather than the gel state.

In the quantitative aspect, adsorption masses at different surface potentials have been measured by the combination of surface/interface measurement instruments and electrochemical control method. For example, electrochemical quartz crystal microbalance (E-QCM) can provide information on mass and structural changes associated with electron transfer as well as adsorption and desorption. In 1996, Lei et al. [35] researched the adsorption process of iodide on Au (111) electrode by using E-QCM. They thought that the change of electrode mass was due to the adsorption or desorption of iodide ions and water molecules on the surface. In 2011, He et al. [36] tested the relationship between the mass changes and the potential of a quartz crystal plate coated with a stainless steel film in 1 mM SDS solution. The mass variation per unit area was about 120 $ng/cm^2$ in 1 mM SDS solution under the step potential changing from 0.03 to –0.4 V. Ellipsometric measurement is an optical method sensitive to monolayer adsorption films. The measurements were taken at different locations on the surface, and the ellipsometric angles were recorded via the nulling ellipsometry principle. In 2015, Zhang et al. [37] used ellipsometry to visualize the molecular gradient of adsorbed SDS on different positions of a bipolar electrode. At the cathodic pole, the adsorbed SDS was desorbed by electrostatic repulsion, while at the anodic pole, the adsorption process was enhanced with the adsorbed mass about 20–30 $ng/cm^2$.

According to the above results, positive potentials can promote the formation of the condensed adsorption film of the anionic surfactant (e.g., SDS) on the surface of different metals in aqueous solution. Comparing with the desorption state under the negative potential of the metal electrode, the mass per unit area under the positive potential can reach about 120 $ng/cm^2$. Of course, the concentration of the surfactant will also influence the adsorption state on the surface of the metal, and further influence the boundary lubrication behavior during the friction tests. These relevant results on the adsorption behavior of the surfactant under electric field are consistent with the present work, well support the results of the wear maps in Figs. 2, 4, and 6. Furthermore, these results also indicate that in the presence of an external electric field, the adsorption behavior of molecules or ions at the metal–aqueous interface can be well regulated without corrosion or corrosive wear.

## 4.2 Effect of electric fields on boundary film and wear particle formation

After the discussion on the adsorption behavior of surfactants under different potentials in the absence of external force, the effects of surface potentials on the surfactant boundary film during friction test will be further introduced. Electrical behaviors of interface between friction pairs and the contact area had been widely used since the 1940s [38]. By combining the contact resistance with COF, we have designed an experiment to analysis the adsorption film formation and failure on the surface of 316L stainless steel plate when rubbing against 304 stainless steel ball under different applied electrical fields. Figure 11(a) presents the model of the experimental setup, which merges a tribometer (UMT-3), a direct-current power supply (two electrodes system), and a contact resistance measuring instrument with the sampling frequency of 100 points per minute. The pressure was about 804 MPa and reciprocating speed about 6 mm/s. Figure 11(b) shows the relationship between the COF and contact resistance verse time. In the first 100 s, no lubricant was added. Propylene carbonate (PC, a kind of ester oil) and PC solution mixed with SDS were added into the contact area at 100 and 300 s, respectively. For the PC with SDS as lubricant, a negative or positive voltage of 10 V was applied, with the lower friction pair of 316L as the work electrode and an external titanium plate as the counter electrode. The positive voltage presented that the work electrode was contacted with the positive pole. Each stage of the voltage control was set to 200 s.

The curves in Fig. 11(b) show that the contact resistance of the 316L plate and 304 ball under the dry friction was about 10 Ω. When pure PC was added as lubricant, the COF decreased from 0.79 to 0.49, while the contact resistance remained almost constant. When PC solution with SDS was added, the COF further decreased to 0.14 and the contact resistance increased to about 100 Ω. When a negative potential of 10 V was applied on the surface of the lower friction pair, the COF increased to ~0.34. When
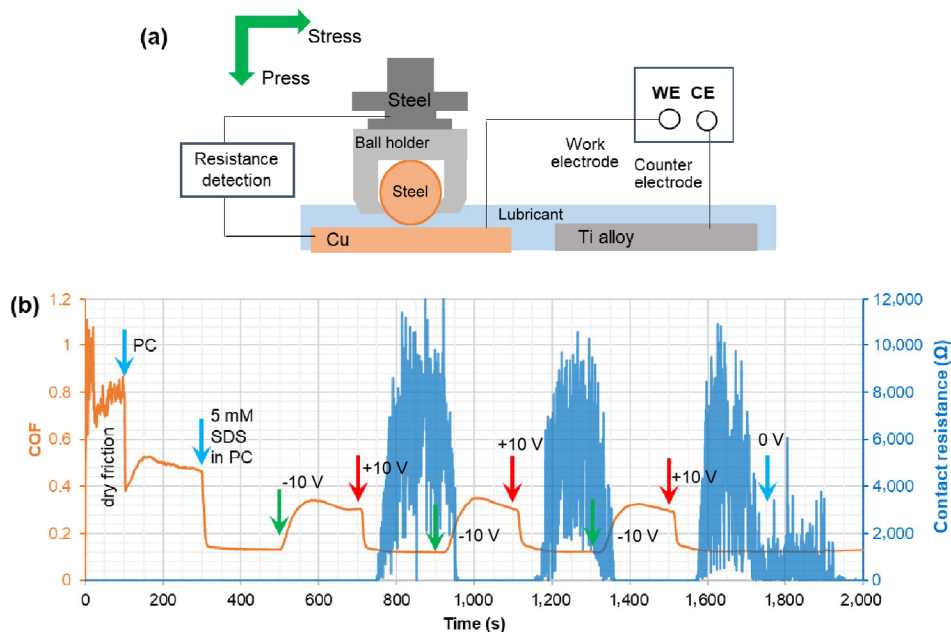
**Fig. 11** (a) Schematic diagram of a tribometer combined with a two electrodes system and a contact resistance measuring instrument, (b) COF and contact resistance vs. time under different lubrication conditions and applied voltages.

a positive potential of 10 V was applied, the COF decreased to 0.12, and the contact resistance obviously increased to 1–10 kΩ.

These phenomena indicated that the addition of SDS decreased the actual contact area between the steels, resulting the obviously decrease of COF. While, the increase of contact resistance was not obvious because of some remaining local actual contact area. Only when the positive potential was applied, a relatively complete boundary film was formed, which resulted in the significantly increase of the contact resistance. On the contrary, at the initial stage of boundary film failure, the change of contact resistance was more quickly than that of COF [39].

Potential controlled adsorption film can not only manipulate the COF, but also regulate the formation of wear particles. According to the fracture-induced adhesive wear criterion proposed by Cao et al. [40], work of adhesion plays a vital role in adhesive wear, especially for metals. The work of adhesion of the metal surface can be well controlled by the adsorption state of surfactant. Given this perspective, we observed the morphologies of the wear particles near the track of lower friction pair under different surface potentials. 316L stainless steel plate and bearing steel ball were used as friction pairs, with 0.025 mM SDS aqueous solution or 0.2 mM SDS PC solution as lubricant. The

pressure is about 880 MPa and reciprocating speed about 10 mm/s. After the friction test of 900 s, the track on the surface of the lower friction pair was observed in the lubricant. Meanwhile, the wear particles distributed near the track were also inspected on an optical microscope (Keyence, Japan) and statistically measured by the software of Image-Pro Plus. Figure 12 shows the processes including track observation, wear particles observation, recognition, and their size statistics.

Under the negative potential of 0.6 V for the lower friction pair, the coverage of the boundary film composed of SDS was not good. The COF value was higher than 0.5. The number of wear particle was more than 1,000, with the average size of 2–6 μm. When the surface potential was +0.4 V, the COF as about 0.10, the wear was slight, and almost no visible wear particles were observed. The mechanism is that SDS boundary film can avoid the direct contact between rough peaks, so that shear occurs in boundary film or between boundary film and solid. In the above boundary lubrication system, the surface or interface properties (including the surface energy influenced by surface adsorption film or surface chemical reactions) of the system are the major factors, rather than the properties of the solid phase (hardness of the friction pairs, viscosity of liquid bulk phase, etc.).
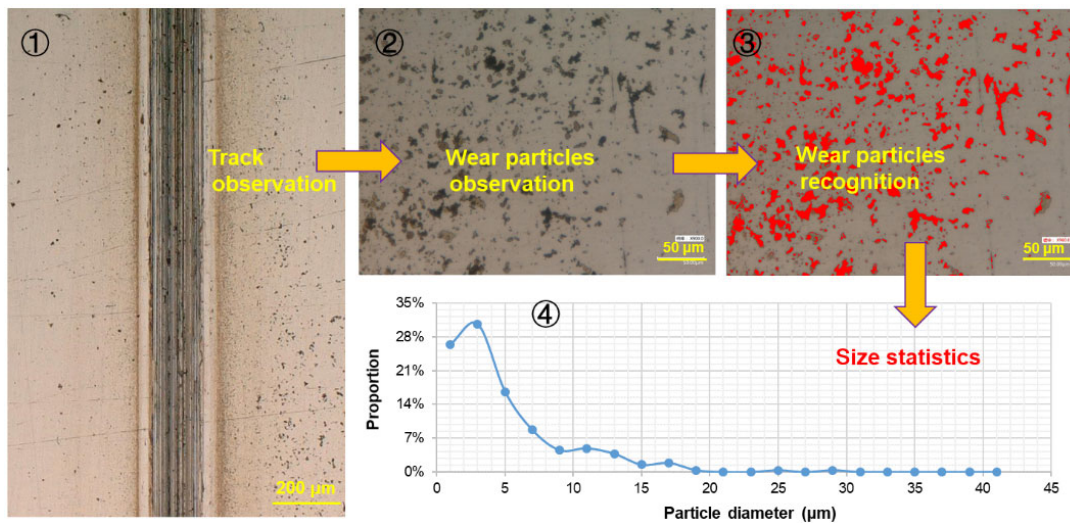
**Fig. 12** Processes of wear particle size observation in the lubricant and its statistics analysis result.

## 4.3 Corrosion resistance and semiconductor properties of adsorption film

Besides the boundary lubrication effect, adsorption film composed of surfactant usually exhibits good corrosion resistance. Ying [41] has reported a method to prepare a monomolecular octadecanethiol layer on the surface of silver coins by ultrasonic bathing. He found that the formed self-assembled, closely packed film illustrated excellent anti-tarnish properties. With this layer, the die life increased three times.

As we know, the nature of corrosion of metals is the exchange of electrons. If the adsorption film composed of surfactants can inhibit the electron exchange between metal and aqueous, it can play a positive effect on corrosion resistance. In 1997, Reed et al. [42] realized the direct observation of charge transport through molecules of benzene-1,4-dithiol by self-assembled on the two facing gold electrodes of a mechanically controllable break junction (MCBJ). Current–voltage measurements at room temperature demonstrated that the threshold resistance of a single molecule was ~22 MΩ. The method provides substantial insight for the study of the electronic properties of single molecules.

Conductive probe AFM can be also used to study the electrical behaviors of surfactants adsorbed on the surface of conductors or semiconductors. Yamada et al. [43] reported the transport properties of self-assembled monolayer on the surface of GaAs by conductive probe AFM. According to their current–voltage characteristics, they found that octadecanethiol functioned as a tunnel barrier and benzenethiol was conductive due to the presence of π-electrons. The results indicate that novel device structures can be designed by selecting functional surfactant molecules and controlling the electronic states of solid-surfactant interface.

## 5  Conclusions

All experimental results which have been presented in this article demonstrate that tribocorrosion and corrosive wear can be mitigated simultaneously and friction coefficient can be sustained at a low level in an appropriate surface potential range, which deviates from the conventional way of knowledge regarding the effect of external electric fields on corrosion and corrosive wear. The key factor in determining the electron transportation across the double electric layer at the solid–liquid interface is the adsorption of ions or charged particles in the window of electrochemical potentials. The adsorption film composed of the surfactant in the aqueous solution has semiconductor properties on the metal surface, which can inhibit electron exchange and improve corrosion resistance of metals. Charging and discharging processes corresponding to adsorption and desorption are considered to be the characteristics of electrochemical potential window, which is considered as the essential

divergence from electrochemical reactions. Meanwhile, surface potential or external electric fields can regulate the concentration and state of the adsorbed surfactant molecule on the metal surface, so as to realize the active control of boundary lubrication and corrosive wear behaviors. Most importantly, by changing the adsorption film state at the solid–liquid interface, external electric field can regulate the interface properties in real time, providing a smart technique for tuning corrosion, friction, and wear behaviors of machine elements at molecular scale.

## Acknowledgements

## References

[1] Mischler S. Triboelectrochemical techniques and interpretation methods in tribocorrosion: A comparative evaluation. *Tribol Int* **41**: 573 (2008)

[2] Poopov Y A. Metals in passive state. *Prot Met* **40**: 568 (2004)

[3] Seyeux A, Maurice V, Marcus P. Oxide film growth kinetics on metals and alloys: I. Physical model. *J Electrochem Soc* **160**: C189 (2013)

[4] Mate C M. *Tribology on the Small Scale: A Bottom up Approach to Friction, Lubrication, and Wear*. Oxford (UK): Oxford University Press, 2008.

[5] Abd-El-Kader H, El-Raghy S M. Wear-corrosion mechanism of stainless steel in chloride media. *Corros Sci* **26**: 647 (1986)

[6] Favero M, Stadelmann P, Mischler S. Effect of the applied potential of the near surface microstructure of a 316L steel submitted to tribocorrosion in sulfuric acid. *J Phys D* **39**: 3175 (2006)

[7] Tan L, Wang Z, Ma Y, Yan Y, Qiao L. Tribocorrosion investigation of 316L stainless steel: The synergistic effect between chloride ion and sulfate ion. *Mater Res Express* **8**: 86501 (2021)

[8] Yan Y, Neville A, Dowson D, Williams S. Tribocorrosion in implants-assessing high carbon and low carbon Co–Cr–Mo alloys by *in situ* electrochemical measurements. *Tribol Int* **39**: 1509 (2006)

[9] Sun Y, Bailey R. Effect of applied cathodic potential on friction and wear behavior of CoCrMo alloy in NaCl solution. *Lubricants* **8**: 101 (2020)

[10] Sun Y, Dearnley P A. Tribocorrosion behavior of duplex S/Cr(N) and S/Cr(C) coatings on CoCrMo alloy in 0.89% NaCl solution. *Journal of Bio- and Tribo-Corrosion* **1**: 2 (2015)

[11] Akonko S, Li D Y, Ziomek-Moroz M. Effects of cathodic protection on corrosive wear of 304 stainless steel. *Tribol Lett* **18**: 405 (2005)

[12] Sun Y, Song C, Liu Z, Li J, Wang L, Sun C, Zhang Y. Tribological and conductive behavior of Cu/Cu rolling current-carrying pairs in a water environment. *Tribol Int* **143**: 106055 (2020)

[13] Xie G, Luo J, Guo D, Liu S, Li G. Damages on the lubricated surfaces in bearings under the influence of weak electrical currents. *Sci China: Technol Sci* **56**: 2979 (2013)

[14] Mohammad A E K, Wang D. Electrochemical mechanical polishing technology: Recent developments and future research and industrial needs. *Int J Adv Manuf Technol* **86**: 1909 (2016)

[15] Kulkarni M, Ng D, Baker M, Liang H, Her R. Electropotential-stimulated wear of copper during chemical mechanical planarization. *Wear* **263**: 1470 (2007)

[16] Zhu Y Y, Kelsall G H, Spikes H A. The influence of electrochemical potentials on the friction and wear of iron and iron oxides in aqueous systems. *Tribol trans* **37**: 811 (1994)

[17] Spikes H A. Triboelectrochemistry: Influence of applied electrical potentials on friction and wear of lubricated contacts. *Tribol Lett* **68**: 90 (2020)

[18] Meng Y, Liu C. Spatiotemporal manipulation of boundary lubrication by electro-charging and electrochemical methods. In *Superlubricity (Second Edition)*. Erdemir A, Martin J M, Luo J, Ed. Elsevier, 2021: 499.

[19] Jiang H, Meng Y, Wen S. Effects of external D.C. electric fields on friction and wear behavior of alumina–brass sliding pairs. *Science in China (Series E)* **41**: 617 (1998)

[20] Chang Q, Meng Y, Wen S. Influence of interfacial potential on the tribological behavior of brass/silicon dioxide rubbing couple. *Appl Surf Sci* **202**: 120 (2002)

[21] He S, Meng Y, Tian Y, Zuo Y. Response characteristics of the potential-controlled friction of $ZrO_2$/stainless steel tribopairs in sodium dodecyl sulfate aqueous solutions. *Tribol Lett* **38**: 169 (2010)

[22] Liu C, Tian Y, Meng Y. A chemical potential equation for modeling triboelectrochemical reactions on solid–liquid interfaces. *Front Chem* **9**: 650880 (2021)

[23] Bard A J, Faulkner L R. *Electrochemical Methods: Fundamentals and Applications*. Hoboken (USA): John Wiley & Sons, Inc., 2001.

[24] Laidler K J, Meiser J H. *Physical Chemistry*. Boston (USA): Houghton Mifflin Company, 1999.

[25] Helmholtz H. Studien über elektrische Grenzschichten. *Ann Phys* **7**: 337–382 (1879)

[26] Stern O. Zur Theorie der elektrolytischen Doppelschicht. *Z. Elektrochemie* **30**: 508 (1924)

[27] Liu C, Fang J, Wen X, Tian Y, Meng Y. Active control of boundary lubrication of ceramic tribo-pairs in sodium dodecyl sulfate aqueous solutions. *Tribol Lett* **69**: 144 (2021)

[28] Zhang J, Meng Y. Stick-slip friction of stainless steel in sodium dodecyl sulfate aqueous solution in the boundary lubrication regime. *Tribol Lett* **56**: 543 (2014)

[29] Su Y. Enhanced boundary lubrication by potential control during copper wire drawing. *Wear* **210**: 165 (1997)

[30] Sotiropoulos S, Nikitas P, Papadopoulos N. Adsorption of sodium dodecylsulphate on mercury as an example of micellization within a multilayer interphase. *J Electroanal Chem* **356**: 201–223 (1993)

[31] Manne S, Gaub H E. Molecular organization of surfactants at solid–liquid interfaces. *Science* (American Association for the Advancement of Science). **270**: 1480 (1995)

[32] Burgess I, Jeffrey C A, Cai X, Szymanski G, Galus Z, Lipkowski J. Direct visualization of the potential-controlled transformation of hemimicellar aggregates of dodecyl sulfate into a condensed monolayer at the Au (111) electrode surface. *Langmuir* **15**: 2607 (1999)

[33] Burgess I, Zamlynny V, Szymanski G, Lipkowski J, Majewski J, Smith G, Satija S, Ivkov R. Electrochemical and neutron reflectivity characterization of dodecyl sulfate adsorption and aggregation at the gold–water interface. *Langmuir* **17**: 3355 (2001)

[34] Leitch J J, Collins J, Friedrich A K, Stimming U, Dutcher J R, Lipkowski J. Infrared studies of the potential controlled adsorption of sodium dodecyl sulfate at the Au (111) electrode surface. *Langmuir* **28**: 2455 (2012)

[35] Lei H, Uchida H, Watanabe M. Electrochemical quartz crystal microbalance study of adsorption of iodide on highly ordered Au (111). *J Electroanal Chem* **413**: 131 (1996)

[36] He S, Meng Y, Tian Y. Correlation between adsorption/desorption of surfactant and change in friction of stainless steel in aqueous solutions under different electrode potentials. *Tribol Lett* **41**: 485 (2011)

[37] Zhang J, Meng Y, Yu X. Control of friction distribution on stainless steel surface in sodium dodecyl sulfate aqueous solution by bipolar electrochemistry. *Tribol Lett* **59**: 43 (2015)

[38] Archard J F. Contact and rubbing of flat surfaces. *J Appl Phys* **24**: 981 (1953)

[39] Liu C, Li X, Li X, Li W, Tian Y, Meng Y. On-line feedback control of sliding friction of metals lubricated by adsorbed boundary SDS films. *Lubricants* **10**: 148 (2022)

[40] Cao H, Tian Y, Meng Y. A fracture-induced adhesive wear criterion and its application to the simulation of wear process of the point contacts under mixed lubrication condition. *Facta Univ Ser: Mech* **19**: 23 (2021)

[41] Ying T. An advanced anti-tarnish process for silver coins and silverware-monomolecular octadecanethiol protective film. *Tribol Trans* **64**: 341 (2021)

[42] Reed M A, Zhou C, Muller C J, Burgin T P, Tour J M. Conductance of a molecular junction. *Science* **278**: 252 (1997)

[43] Yamada F, Shirasaka T, Fukui K, Kamiya I. Surface state control of III−V semiconductors using molecular modification. *Phys E* **42**: 2841 (2010)

**Chenxu LIU.** He received his Ph.D. degree from Department of Mechanical Engineering, Tsinghua University, China, in 2021. He is currently a post-doctor at State Key Laboratory of Tribology in Advanced Equipment, Tsinghua University, China. His research interests include potential controlled boundary lubrication and tribo-electrochemistry.

**Yonggang MENG.** He is a professor in mechanical engineering at State Key Laboratory of Tribology in Advanced Equipment, Tsinghua University. He received his M.S. and Ph.D. degrees from Kumamoto University, Japan, in 1986 and 1989, respectively. His current research interests cover modeling of friction, wear and lubrication in macro/micro-tribosystems and its applications to tribological design of machine elements.